A global monthly climatology of total alkalinity: a neural network approach

Daniel Broullón[1], Fiz F. Pérez[1], Antón Velo[1], Mario Hoppema[2], Are Olsen[3], Taro Takahashi[4], Robert M. Key[5], Melchor González-Dávila[6], Toste Tanhua[7], Emil Jeansson[8], Alex Kozyr[9] and Steven M.A.C. van Heuven[10]

[1]Instituto de Investigaciones Marinas, CSIC, Eduardo Cabello 6, 36208 Vigo, Spain

[2]Alfred Wegener Institute Helmholtz Centre for Polar and Marine Research, Postfach 120161, 27515 Bremerhaven, Germany

[3]Geophysical Institute, University of Bergen and Bjerknes Centre for Climate Research, Allègaten 70, 5007 Bergen, Norway

[4]Lamont-Doherty Earth Observatory of Columbia University, Palisades, NY 10964, USA

[5]Atmospheric and Oceanic Sciences, Princeton University, 300 Forrestal Road, Sayre Hall, Princeton, NJ 08544, USA

[6]Instituto de Oceanografía y Cambio Global, IOCAG, Universidad de Las Palmas de Gran Canaria, Las Palmas de Gran Canaria, Spain

[7]GEOMAR Helmholtz Centre for Ocean Research Kiel, Düsternbrooker Weg 20

D-24105 Kiel, Germany

[8]Uni Research Climate, Bjerknes Centre for Climate Research, Jahnebakken 5, 5007 Bergen, Norway

[9]NOAA National Centers for Environmental Information, 1315 East-West Hwy Silver Spring, MD 20910 USA

[10]Faculty of Science and Engineering, Isotope Research – Energy and Sustainability Research Institute Groningen, University of Groningen, Nijenborgh 6, 9747 AG Groningen, The Netherlands

Correspondence to: Daniel Broullón (dbroullon@iim.csic.es)

Abstract. Global climatologies of the seawater CO_2 chemistry variables are necessary to assess the marine carbon cycle in depth. The seasonal variability should be adequately captured in them to properly address issues such as ocean acidification. Total alkalinity (A_T) is one variable of the seawater CO_2 chemistry system involved in ocean acidification and frequently measured during campaigns assessing the marine carbon cycle. We took advantage of the data product Global Ocean Data Analysis Project version 2 (GLODAPv2) to extract the relations between the drivers of the A_T variability and this variable

using a neural network to generate a monthly climatology. 99% of the GLODAPv2 dataset used was modelled by the network with a root-mean-squared error (RMSE) of 5.1 µmol kg^{-1}. The validation carried out using independent datasets revealed the good generalization of the network. Five ocean time-series stations used as an independent test showed an acceptable RMSE

30   in the range of 3.1-6.2 µmol kg^{-1}. The successful modeling of the monthly variability of A_T in the time-series makes our network a good candidate to generate a monthly climatology. It was obtained passing the climatologies of the World Ocean Atlas 2013 (WOA13) through the network. The spatiotemporal resolution of the climatology is determined by the one of WOA13: 1°x1° in the horizontal, 102 depth levels (0-5500m) in the vertical, and 12 months. We offer the product as a service to the scientific community at the data repository of the Spanish National Research Council (CSIC; doi:

35   http://dx.doi.org/10.20350/digitalCSIC/8564) with the purpose to contribute to a continuous improvement of the understanding of the global carbon cycle.

1 Introduction

The marine carbon cycle is a key elemental cycle of the ocean and, by virtue of its interaction with the atmospheric carbon

40   dioxide, of fundamental significance for the Earth's climate (Tanhua et al., 2013). The capacity of the ocean to dissolve atmospheric CO_2 and to store it, and the chemical speciation after its dissolution, has permitted to maintain approximately 30% less CO_2 in the atmosphere (Le Quéré et al., 2017) than it would contain due to anthropogenic emissions. Nevertheless, this service of the ocean to slow down the consequences of the climate change has led to a major problem: ocean acidification (Doney et al., 2009). The main change in the ocean chemistry that defines this phenomenon is the progressive decrease of

45   seawater pH with the increase in anthropogenic CO_2. Together with other changes associated with climate change (e.g., increase in temperature), this process could have severe consequences for marine ecosystems (Orr et al., 2005; Fabry et al., 2008; Hoegh-Guldberg and Bruno, 2010; Kroeker et al., 2013) and, consequently, for life on our planet.

Detailed spatiotemporal knowledge about the inorganic chemistry of the marine carbon cycle is necessary to understand this challenging problem and to evaluate it properly. The seawater CO_2 chemistry can be described by four variables: total alkalinity

50   (A_T), total dissolved inorganic carbon (TCO_2, also known as DIC), partial pressure of CO_2 (pCO_2) and pH. A_T is a key variable in the framework of ocean acidification because of what it represents: the capacity of the ocean to buffer the changes in pH.

The global ocean distribution of A_T is a result of different physical and biogeochemical processes that change the concentration of the ionic species (Wolf-Gladrow et al., 2007) that shape A_T. Processes that change salinity are the most important for changes in surface A_T, which is shown through the strong linear correlation of salinity and A_T (Millero et al., 1998; Takahashi

55   et al., 2014). Therefore, in the surface layer precipitation and evaporation are the physical processes that control most of the distribution of A_T. Rivers can affect marine A_T locally, related to the magnitude of runoff and the A_T carried by them

(Hoppema, 1990; Anderson, 2004; Cooper et al., 2008). The formation and dissolution of carbonate minerals also have an important contribution to the variability of A_T (Fry et al., 2015). Connected with the dissolution of carbonate at depth, the variability in upwelling areas is also controlled by the supply of subsurface waters with high A_T (Fine et al., 2017). Finally,

60 the organic matter cycle contributes to changes of A_T through the consumption and regeneration of nutrients and oxygen (Brewer and Goldman, 1976; Wolf-Gladrow et al., 2007).

In addition to the spatial variability, all the drivers mentioned above generate seasonal A_T variability. For example, phytoplankton blooms (i.e., primary production), and the seasonality in upwelling and river flows. Even though A_T is the variable of the seawater CO_2 chemistry system with the least seasonal variability (Lee et al., (2006) estimated a range from

65 near 0 up to 80 μmol kg^{-1}), it is important to take it into account because of the importance of this variable in the storage of the anthropogenic carbon in the ocean and in the buffering of changes in the seawater pH. Therefore, the knowledge of A_T variability over the global oceans at monthly timescales is very useful to increase the understanding of the ocean carbon cycle and to make assessments and projections related to ocean acidification with greater rigor.

High-quality data is a crucial first requirement to address the problem. Ocean time-series data represent excellent records to

70 study the seasonality of the ocean carbon cycle as well as its inter-annual trends (e.g., Bates et al., 2014). Unfortunately, there are only a few time-series that include highly precise measurements of the seawater CO_2 chemistry at seasonal resolution and they are only representative of small areas. Alternatively, different global data products have been released for public usage in recent years. The main ones for the ocean surface are the Surface Ocean CO_2 Atlas (SOCAT; Bakker et al., 2016) and the Lamont-Doherty Earth Observatory database (LDEO; Takahashi et al., 2016). Both data products are complementary, offer

75 annual updates and include tens of millions of pCO_2 measurements in the global ocean. For the interior ocean, a comprehensive and global database and data product was recently made public: Global Ocean Data Analysis Project version 2 (GLODAPv2) (Key et al., 2015; Olsen et al., 2016). This quality-controlled collection contains thousands of measured data of seawater CO_2 chemistry variables over the full water column from more than 700 cruises conducted in all regions of the global oceans during the last four decades.

80 The logical next aim will be to generate a globally consistent climatology for the different variables. The seasonal variability should be captured correctly in it. Different approaches have been carried out to fill the spatial and temporal gaps in the observations of A_T to generate a global seasonal climatology. Lee et al. (2006) grouped A_T data (< 20-30 m depth) into 5 oceanographic regimes and obtained a best fit to a quadratic function of sea surface temperature (SST) and sea surface salinity (SSS) in each basin. Takahashi et al. (2014) divided the global ocean into 33 hydrographic provinces and expressed the

85 potential alkalinity (PALK = A_T + NO$_3^-$, < 50 m depth) as a linear regression of salinity in 27 of them. PALK was used instead of A_T for the purpose of eliminating seasonal biological effects, and the inter-province variation reflected differences in $CaCO_3$ production in the mixed layer as well as the contributions of lateral and vertical mixing of waters. These studies only cover the

surface ocean. However, a robust climatology of the entire water column is necessary for models to attain a higher level of evaluation.

90   In this study, we present a global monthly climatology for A_T in a 1°x1° grid with the upper 102 standard depth levels (0-5500m) of the World Ocean Atlas 2013 (WOA13). We have used the high potential of neural network techniques to achieve this objective. Similar approaches have demonstrated the capability of these artificial intelligence techniques to learn relationships between predictors and seawater CO_2 chemistry variables and use them to reconstruct global pCO_2 variability at monthly resolution over the last few decades (e.g., Landschützer et al., 2013, 2014). The climatology of A_T presented here

95   takes advantage of the large number of recently available measurements and the ability of the neural networks to capture and include the surrounding natural variability. Additionally, we were able to reduce the error reached with the relations obtained by the previous efforts to build a seasonal climatology of A_T (Lee et al., 2006; Takahashi et al., 2014) and to extend them deeper into the water column.

2 Methodology

100   A feed-forward neural network was configured to compute A_T throughout the global ocean and to create a monthly climatology. It was chosen based on the good ability to learn the relationships between A_T and the variables related to its spatiotemporal variability as shown in Velo et al. (2013).

The feed-forward neural networks are composed of layers: the input layer, a variable number of hidden layers and the output layer (Fig. 1). The input layer is a matrix representing the entry to the network of the data from which the outputs are going to

105   be obtained. The hidden and output layers are composed of an adjustable number of neurons. These latter elements are formed by a series of weights, a bias, a summation, and a transfer function (Russell and Norvig, 2010) and they are the connections between the layers. A neuron receives all the outputs of the previous layer and multiplies them by a matrix of weights. Then, these results are summed and a bias is added. Finally, the transfer function is applied over the sum and an output is obtained from each neuron.

110   The ability of the network to produce a desired output stems from a training process. Given a set of inputs and their targets, the network is trained to learn the relationships between both sets. The training process is possible due to a backpropagation training algorithm (Rumelhart et al., 1986). Generally, the network is initialized with random values of weights and biases and an output is obtained. This output is compared with the target through a cost function, which typically is the mean squared error. Then, the algorithm "backpropagates" this error through the network and iteratively adjusts the weights and biases to

115   minimize the cost function. The minimization is commonly based on the Levenberg-Marquardt algorithm (Levenberg, 1944; Marquardt, 1963). Once the network is trained, output values can be accurately obtained from a set of inputs with unknown targets.

The feed-forward neural network used in this study has a two-layer architecture. The first layer has a sigmoid transfer function and the second layer a linear transfer function (Fig. 1). This choice of functions allows both the linear and non-linear

120   relationships between A_T and its predictors to be represented by the network. This network configuration is able to approximate most functions arbitrarily well (Hagan et al., 2014). In the Atlantic Ocean, this arrangement allowed to obtain a model to accurately calculate the A_T from diverse predictors (Velo et al., 2013).

The GLODAPv2 dataset was used to train the network. The input variables to the network (left hand in Fig. 1) were selected based on their potential influence on the A_T, as previously described. They include the sampling position (coordinates and

125   depth), potential temperature, salinity, nutrients (phosphate, nitrate and silicate) and dissolved oxygen. The position was included to help the network to learn characteristic patterns associated with this input when the other variables cannot fully explain the A_T. Takahashi et al. (2014) and Lee et al. (2006) showed how the relations between A_T and the predictor variables used in these studies are different depending on the ocean area. The periodicity of the input longitude was represented by the equations used by Zeng et al. (2014):

130
$$clon = \cos\left(\frac{\pi}{180} \cdot longitude\right)$$

$$slon = \sin\left(\frac{\pi}{180} \cdot longitude\right)$$

Our approach only uses measured inputs from GLODAPv2, that is, those input data derived from the same Rosette sample bottle as the A_T value. Other studies with a similar approach take the inputs from reanalysis products or satellite data (e.g.,

135   Landschützer et al. 2013), which in general are less accurate than direct measurements. The relations created by the network in the training procedure are likely to be more realistic using in situ measured values for the input variables.

The samples where all input variables and A_T were measured were selected from GLODAPv2 (https://www.nodc.noaa.gov/ocads/oceans/GLODAPv2/). From these, we removed one record due to its spurious oxygen value. Moreover, we excluded the data of the ocean time-series from the training procedure to use them in an independent

140   validation. The final dataset used in this study contained 246,221 samples.

Two different training techniques were tested: the Levenberg-Marquardt method and the Bayesian Regularization (MacKay, 1992). In a similar approach, Velo et al. (2013) demonstrated that these techniques give the best network performance. The number of neurons in the network is problem dependent and there is no fixed criterion to establish it. It is related to the complexity of the input-output mapping, the amount of training data available and their noise (Gardner and Dorling, 1998).

145   Using too few neurons will not enable to learn complex relations. Using too many neurons could overfit the data, that is, the network might model the uncertainty of the data used in the training. Here, we determine the optimal number of neurons

through a trade-off between the root-mean-squared error (RMSE) of the computed values and the generalization of the network. This last concept refers to the performance of the network when a set of unused inputs in the training procedure is introduced in the network to obtain an output. If the RMSE in this set is of the same order of magnitude as the RMSE in the training set,

150   there is no substantial overfitting and the network generalizes well.

The training procedure was carried out in MATLAB. We tested 32, 64, 128 and 264 neurons in the hidden layer based on the results of Velo et al. (2013). For each number of neurons, we trained 10 networks always using the same 90% of the available data (initial training dataset) and conducted a subsequent independent test always using the same remaining 10% (initial testing dataset). Both datasets contained samples randomly distributed in the ocean to evaluate the maximum possible relations

155   between the input variables and A_T through all oceanographic regimes, that is, to capture most of the variability in all the variables and not restricting the sets to specific areas. The MATLAB training procedure divides by default our initial training dataset in training, validation and testing datasets. Each of the 10 networks starts the training procedure with random weights and biases values and a random division of the data in the three sets. This makes the minimization of the cost function different for each network due to the complexity of the weights-error space and their different starting points. We kept our initial training

160   and testing datasets to evaluate the generalization of each network always in the same data to properly select the best network. Finally, the selected network is the one with the best generalization in the initial testing dataset.

The division of the initial training dataset was made in such a way that 70% is training, 15% validation and 15% testing. Once we found an adequate configuration of the network, we increased the amount of data in the training set to capture more relations between the inputs and A_T. The new percentages of the sets were: 80% training, 20% validation and 0% testing. The latter set

165   is only necessary to evaluate the overfitting. As we evaluated it in the previous step, we decided to omit it to have more data in the training set. However, we kept our initial testing dataset to evaluate each of the 10 networks in the same way.

In a last step to improve the network mapping, we retrained the selected neural network in the same way as described above but without the samples with a difference between measured and computed A_T (residuals) beyond ±3RMSE. We followed this statistical criterion to identify ocean regions where the network is not able to obtain accurate values and to improve the network

170   mapping in the other areas.

To illuminate the complexity of neural networks, several methods to determine the contribution of each predictor variable in the output were proposed in different studies (see Gevrey et al. (2003) and Olden et al. (2004)). We used the Connection Weight Approach (Olden and Jackson, 2002) to evaluate if the network properly associates the variability of the A_T with the predictor variables. This method was proposed to be the most accurate (Olden et al., 2004). It uses the weights obtained in the

175   training stage to extract the influence of each predictor variable in fitting the A_T values. The expression followed was:

$$C_i = \sum_{k=1}^{H} w_{ik} \cdot w_k$$

where C_i is the relative importance of the predictor variable i, H is the number of neurons in the hidden layer, w_{ik} is the weight of the connection between the variable i and the neuron k of the hidden layer and w_k is the weight of the connection between the neuron k of the hidden layer and the final output, that is, the computed A_T. Finally, the absolute value of C_i was expressed

180   as a percentage of the sum of all C_i.

The potential of the network was also tested to a greater extent than in the GLODAPv2 testing dataset on five ocean time-series in different oceanographic regimes: Hawaii Ocean Time-Series (HOT), Bermuda Atlantic Time-Series Study (BATS), European Station for Time-Series in the Ocean at the Canary Islands (ESTOC), Kyodo North Pacific Ocean Time-Series (KNOT) and K2.

185   The GLODAPv2 dataset contains quality controlled oceanographic measurements in all ocean basins from the 1970s until 2013 (Olsen et al., 2016). While coverage is global, winter data are scarce or even more or less absent in some high latitude regions because adverse weather conditions prevents field activities in that season (Fig. 2). This temporal bias could be solved with the help of the data of the subsurface layer and below it from the seasons with sufficient samples. Vázquez-Rodríguez et al. (2012) demonstrated how the subsurface ocean layer in the Atlantic Ocean can retain the footprint of the water mass

190   formation from the preceding winter in the following months and, therefore, of the surface conditions. Furthermore, the physical-chemical properties in this layer and below it, have a low or even null seasonal variability. Thus, the winter relationship between inputs and A_T that we need for producing an all-season reliable climatology with the neural network are mostly preserved in this subsurface layer and below it at other times. The validity of this hypothesis was tested in other regions (Fig. 2) following Vázquez-Rodríguez et al. (2012).

195   Finally, we generated a 1°x1° global monthly climatology of A_T on 102 depth levels from the objectively analyzed climatological fields of WOA13 (Locarini et al., 2013; Zweng et al., 2013; Garcia et al., 2014a; Garcia et al., 2014b). From this database, the same input variables as in the training stage were selected to estimate A_T from the relationships learned by the network. This final product was compared with the monthly sea surface climatologies of A_T of Lee et al. (2006) and Takahashi et al. (2014). Furthermore, the annual mean was compared with the annual mapped climatology by Lauvset et al.

200   (2016). The availability in Lauvset et al. (2016) of the climatologies of the variables used as inputs in the network were used to test how the network represents their climatology of A_T and to evaluate the sources of the possible differences.

3 Results and discussion

3.1 Neural network analysis

The optimal number of neurons was found to be 128. The similar value of the RMSE reached for the training set and the testing

205 set (8 µmol kg^{-1} vs 8.5 µmol kg^{-1}; Fig. S1) shows that no overfitting occurred, and the network generalizes well. The two training techniques used did not show significant differences (Table 1). The Levenberg-Marquardt algorithm was selected for its higher computing speed. We also found no improvement by increasing the amount of data points in the training set. The main reason is perhaps the random division of the datasets. All possible relations the network can learn could be represented using only 70% of the initial training dataset, that is, 63% of the GLODAPv2 dataset used in this study.

210 The samples with residuals beyond ±3RMSE are 1% of the global dataset. In general, the spatial distribution of them (Fig. S2) shows that they are confined to certain areas and the biggest errors are in the surface samples (Fig. 3). The Northern Hemisphere contains almost all these samples (Fig. S2 and Fig. 3). Specifically, 64% of them are from latitudes north of 60ºN (Table S1). They make up 6.5% of all the samples in this zone and 85% of them belong to the upper 100m of the water column (Table S2). Typically, they have salinities lower than 34 (Table S3; Fig. S2). In this layer of this area, the samples with residuals

215 beyond ±3RMSE are 14% of the total. A monthly analysis here shows that the largest number of samples are from the summer months. About 14-18% of all the samples from this season in this area have residuals higher than ±3RMSE (Table S4).

The previous results show that the Arctic Ocean is the region with the largest RMSE although the network computes well most of the measured A$_T$ in this area. However, the low availability of winter data, the ice-sea dynamics and the transport of A$_T$ by the rivers (Fig. S3) could disengage the presence of the surface winter conditions in the summer subsurface layer shown by

220 Vázquez-Rodríguez et al. (2012) in other areas and generate a temporal bias in the climatology. The high discharge of high A$_T$ waters by the rivers in the summer (Fig. S4) promotes the greatest errors in this time showing how the network fails to model riverine A$_T$.

In further detail, many of the samples with residuals beyond ±3RMSE are located in the Beaufort Sea (66°N - 80°N, 140°W-180°W). Here, Takahashi et al. (2014) also found the largest RMSE (60.5 µmol kg^{-1}; 57.6 µmol kg^{-1} applying their regression

225 on GLODAPv2) of their SSS-PALK relations in the upper 50m of the water column. This area is specifically complex for the modeling of surface A$_T$ because of the already mentioned presence of significant river runoff with high and possibly variable A$_T$ concentrations (Fig. S3 and S4; Anderson et al. 2004; Cooper et al. 2008). Therefore, in spite of the good reproduction of the A$_T$ of the majority of the samples, one should be cautious with the resulting data in this zone; this actually holds for the whole Arctic Ocean.

230 The North Sea is the other area that contains a striking number of samples with residuals beyond ±3RMSE. Specifically, the samples shallower than 100m and close to the coasts surrounding this sea do not have a well computed A$_T$ (Fig. S3). Some studies have shown the complexity of the processes occurring in this shallow sea where the high river runoff also has elevated

levels of A$_T$ (Fig. S3; e.g., Hoppema, 1990; Artioli et al. 2012). Hence, the same recommendation as for the Arctic Ocean should be made.

235 In general, the network mainly fails to compute A$_T$ in some samples of areas with rivers carrying significant amounts of A$_T$ to the ocean. The inclusion in the network of new predictors related to the influence of the concentration of the riverine A$_T$ in each training sample could improve the computation in these areas. However, the samples beyond ±3RMSE represent 23% and 9.4% of the total for the Beaufort Sea and the North Sea respectively, above 100m. As an argument for the contrary, most of the samples have a well-computed A$_T$ even in these complex areas. Although one should be cautious, these zones still should

240 be taken into account and be represented in the climatology.

In the global ocean surface layer, the RMSE is lower than the one obtained with the relations of the previous studies on generation of monthly climatologies (Table 2 and 3). Relationships between SST and SSS with A$_T$ by Lee et al (2006) have been shown to produce the lowest RMSE (area-weighted RMSE of 8.1 µmol kg^{-1}) in the A$_T$ computation. Applying the relations of that study to GLODAPv2, the obtained weighted RMSE is higher than the one from the neural network (Table 2).

245 We obtained a better fit in all the areas defined in the study of Lee et al. (2006) (Table 2). NNw3RMSE improves the results obtained with the NN in almost all the regions, being the most remarkable the Equatorial Upwelling Pacific. However, the difference in the weighted RMSE of the two networks is not significant.

Similar to the previous case, the analysis of the error in the areas defined in Takahashi et al. (2014) also shows a better fit of the neural network (Table 3). Except for the zone with the lowest number of samples (Red Sea), the other 26 areas have a

250 lower RMSE when the A$_T$ is computed by a neural network. The NNw3RMSE improves the fitting of the NN in the non-Arctic areas. The zones defined in the Arctic have higher RMSEs in the two studies. As discussed before, the Beaufort Sea is the zone with the highest RMSE. The inclusion of this area in calculating a global RMSE raises its value considerable. The NNw3RMSE has a higher global weighted RMSE because of the exclusion of most of the samples in this area to train this network. However, the weighted RMSE calculated excluding this area shows again a non-significant difference between the two networks (Table

255 3).

The results of the two networks clearly show how this fitting technique computes A$_T$ more accurately than the other methods used in studies on the generation of monthly climatologies. The non-linear nature of the neural networks used in this study and the inclusion of multiple predictor variables related to the A$_T$ variability are the main reasons for a good fit. Furthermore, we only used one neural network for the entire ocean. This has the advantage of obtaining the computed A$_T$ anywhere in the ocean

260 in only one step. No "patches" or smoothing are needed between different zones as in previous climatologies. Finally, the NN has been chosen to generate the climatology. NN3wRMSE better computes A$_T$ in the non-Arctic areas but with a non-significant difference with NN. In order to include the Arctic in the climatology, the better fit in this area with the NN makes

it the best candidate. In any case, the NN3wRMSE is also offered to the users who want to obtain a climatology in a specific area where this network computes A_T better than NN.

265   The NN seems to associate the variability in A_T to the predictor variables in a coherent way. The relative importance of these variables depicted in Fig. 4 shows that salinity is the most influential variable, followed by dissolved oxygen and nutrients. In the surface layer, where the variability of the A_T is the biggest, different studies showed how changes in salinity are highly correlated with this variability (Millero et al., 1998; Takahashi et al., 2014). The organic matter cycle also has a significant component in the variability of the A_T (Kim and Lee, 2009). Dissolved oxygen and nutrients reflect this cycle thought their

270   variations. The network seems to capture this process giving a second place in importance to these variables. The third group of variables in the ranking of importance is comprised by depth and temperature. The former variable could be associated to the variability of the A_T accounting for the variation produced by the $CaCO_3$ cycle and the processes acting through the global ocean circulation. The latter has also been associated to the A_T variability as a proxy of both the $CaCO_3$ and the organic matter cycles (Lee et al., 2006). Finally, the minor contribution of the variables of horizontal sampling position could help to separate

275   the different relations shown by previous studies in different ocean areas (Lee et al., 2006; Takahashi et al., 2014).

3.2 Time-series validation

The network can compute A_T well at different ocean time-series stations. Low RMSEs and high coefficients of determination (r^2) were obtained (Table 4). The bias is relatively low in the three time-series with the highest number of data. The A_T computed by the NN at KNOT and K2 is higher than the measured one. Summed to the previous test, this independent test

280   with a seasonal time resolution shows the good generalization of the NN.

In a similar approach to compute A_T using neural network techniques, Sauzède et al. (2017) found a higher RMSE (7 µmol kg^{-1}) and a lower r^2 (0.95) for the HOT time-series. The absence of nutrients as input in their neural network might explain the better results in our study. The inclusion of nitrate and silicate as predictor in the multilinear regressions performed by Carter et al. (2016) also results in a good fit in the upper 25m of the water column in BATS and HOT (RMSE = 6 µmol kg^{-1} in both

285   time-series). We obtained similar values of RMSE of 6 µmol kg^{-1} and 5.5 µmol kg^{-1} respectively. It appears that using nutrients as a predictor variable of the model improves the A_T computation independent of the approach. The processes related to the influence of the nutrients on the A_T explained previously appear to be captured as it has been shown in the degree of importance of the predictor variables (Fig. 4).

The ability of the network to capture the A_T variability is exemplified in Fig. 5. The other largest time-series also show a good

290   agreement between the computed and the measured seasonal A_T in this surface layer (RMSE HOT: 5.3 µmol kg^{-1}; RMSE ESTOC: 4.2 µmol kg^{-1}). The same holds for other depth layers. In general, the changes in A_T measured in each month of the year are well modeled by the network (inner charts in Fig. 5). Only some extreme values are not fully captured but almost all

the trends between months are well represented. The differences may be caused by a bad quality of the measured A_T or of some of the input variables; they may also be due to an under/overestimation of the network. Furthermore, the time-series

295 areas are not fully represented in all months in GLODAPv2 dataset. However, the network computes A_T in any month with a very low error. This shows again the potential of the generalization of a well-designed neural network.

The network also has the capacity to increase the number of A_T data in the time-series. In many samples, A_T was not measured but the other input variables for the network are available. Therefore, the computed A_T has a higher temporal and spatial resolution. This enables the computation of more reliable trends than with the less frequently measured A_T and allows the

300 identification of possible high frequency changes. The improvement in resolution is especially visible in the longer time-series: HOT and BATS (Fig. 6). In the former we increased the number of A_T data from 3852 to 14089 (Fig. 6b) and in the latter from 3033 to 11342 (Fig. 6b). The error continuity with depth in several profiles might suggest uncertainties in the measurements (Fig. 6c). Alternatively, some processes not properly captured by the network could be taking place at those dates.

3.3 Subsurface Layer Hypothesis

305 We found that the optimal depth range of the subsurface layer defined by Vázquez-Rodríguez et al. (2012) for the North Atlantic Ocean (100-200 m) must be modified in other regions. The area analyzed in the Indian Ocean agrees with that study. However, the other areas show a better verification of the hypothesis if the range is 50-100 m. The different strengths of deep mixing and convection in winter could explain this fact.

The properties analyzed in the four areas defined in Fig. 2 show, as expected, a higher monthly variability in the ocean surface

310 than in the subsurface layers. The intra-annual variability depicted in Fig. 7 should also be typical of a larger region within a similar oceanographic regime for each defined area. The surface winter conditions of the analyzed properties are quite similar to those in the subsurface layer in four consecutive months to winter in all oceans (Fig. 7). In the subsurface layer and below it, the low or hardly any variability allows to retrieve winter conditions in other seasons.

3.4 Climatology

315 The monthly climatology of A_T is based on the relations obtained in the training procedure of the neural network applied to the WOA13 monthly climatological fields. It was demonstrated that the A_T computed by the neural network successfully represents the measured A_T when the inputs associated to it are passed through the network. That is, the relations obtained from GLODAPv2 in the training stage are robust. Therefore, the A_T patterns in the climatology are forced by the patterns of the WOA13 variables used as inputs. A netCDF file can be found at the data repository of the Spanish National Research

320 Council (CSIC; doi: http://dx.doi.org/10.20350/digitalCSIC/8564) together with a video of the monthly variation at the surface and in three longitudinal sections of the three main oceans.

The distribution of the surface annual mean A_T (Fig. 8) is similar to that shown in previous climatologies (e.g., Lee et al. 2006; Takahashi et al. 2014; Lauvset et al. 2016). Not surprisingly, there is a high correlation with the salinity distribution and, consequently, with the evaporation-precipitation patterns. The largest values in the surface layer occur in the Mediterranean

325   Sea, Red Sea, and in the subtropical gyres of the Atlantic and South Pacific Oceans, all of them prevailing throughout the year in the monthly climatology. At depth, these maxima are all present at least up to 150m (Fig. 8). Below 700m, the Pacific and Indian Oceans show higher A_T concentrations than the younger waters of the Atlantic (Fig. 8). Furthermore, features such as the high-A_T Mediterranean Water entering the Atlantic Ocean are captured in the climatology (Fig. 8, 1000m chart, black circle). In general, the patterns agree with the main ocean processes responsible for the A_T variability as explained previously.

330   The seasonal amplitude of sea surface A_T (Fig. 9) is generally in agreement with that obtained by Lee et al. (2006). The highest amplitudes are in the north equatorial zone, in the Arctic Ocean and in coastal zones, i.e., at locations where there are rivers with a large water discharge (like the Amazonas, Congo, La Plata or Arctic rivers). The seasonal amplitude of the surface salinity (Fig. S5) can explain most of the variability in the seasonal amplitude of A_T. In areas with a large seasonal amplitude of salinity (more than 1 unit; mainly the Arctic Ocean and coastal zones near rivers with high discharge), this variable linearly

335   explains 76% of the seasonal amplitude variability of A_T. However, the seasonal amplitude in the Arctic Ocean should be taken with caution due to the difficulty to accurately model this complex zone, as discussed previously. Despite the presence of high levels of A_T in some river mouths in the melting months, the A_T carried by the rivers could be not represented in the climatology and this can enhance the seasonal cycle due to an underestimated value in low salinity waters with high riverine A_T. On the other hand, in areas with a low seasonal amplitude of salinity (less than 1 unit; mainly oceanic areas and coastal

340   regions without rivers with high discharge) about 61% of variability is linearly explained. This fact shows how the network also considers the relations between A_T and the other input variables to explain the A_T variability. Furthermore, the difference in the explained variability between the two areas shows the potential of using sampling position as input.

At depth, the seasonal amplitude of A_T is progressively reduced (Fig. S6). In general, the changes in the variables which influence the changes in A_T are smaller than in the surface layer or null causing this reduction. Below 500m depth level, the

345   seasonality disappears almost completely. The lack of seasonal resolution in the climatologies of nutrients in WOA13 below this level cause the reduction of the variability. Some patches of variability are present likely because of a conjunction of the error of the network and the monthly changes in the other WOA13 inputs. In addition, they could also come from the learning stage since the training data present monthly variations of up to ~10 μmol kg^{-1} for the same area, even at depths greater than 1000m.

350   Although it was shown that the neural network can accurately compute A_T, the quality of WOA13 data determines how robust the climatology is. The climatological values offered here should be evaluated by comparing them with climatological measured data, that is, a monthly average over many years. This can only be done at the locations of time-series with a representative amount of data; Fig. 9 shows this analysis. At both BATS and HOT time-series, the differences between the

climatological measured A_T (Fig. 9, red line) and the climatology (Fig. 9, yellow line) are quite low. Furthermore, when the
355   A_T is obtained by the NN using as input the values of the variables measured at the time-series (Fig. 9, purple line), the results
are even better. The differences of the two comparisons show the differences in the input variables. The climatological
measured data are for the periods between 1991 and 2015 (BATS) and 1989 and 2016 (HOT) and WOA13 data are supposed
to cover a larger range. Despite the difference, the climatology represents quite accurately the measured values averaged in
each month.

360   Compared to the other climatologies, the surface annual mean A_T is more similar to that of Lee et al. (2006) (Table 5). This is
likely because temperature and salinity are included as non-linear predictors of A_T. In Takahashi et al. (2014), A_T derives from
the linear regression between PALK and one predictor and in the Lauvset et al. (2016) study, DIVA spatial interpolation was
used. Furthermore, the coarser grid in the Takahashi et al. (2014) climatology involves a change of grid for the comparisons
which may enhance dissimilarities.

365   The comparison of the monthly values of our climatology and the others available at the same time frequency (Table 6) shows
again the greatest similarity of ours and Lee et al.'s (2006). The reasons given above may also hold here. Part of the differences
between the comparisons may originate from the different versions of the WOA used in each study (Lee et al., 2006:
temperature and salinity from WOA01; Takahashi et al., 2014: salinity from WOA09 and nitrate from WOA94; this study: all
inputs from WOA13).

370   In general, the spatial patterns of the differences between in annual mean surface A_T between our and the three other
climatologies under consideration are not correlated. Compared to Takahashi et al. (2014), the largest differences are in the
Beaufort Sea and in three zonal bands: 54-60º S, 8-28º N and 40-60º N (Fig. S7a). The Pacific Ocean has the highest
dissimilarities in these three bands. In general, the Atlantic Ocean and the Indian Ocean have the smallest differences. The
largest differences in these two ocean basins are mainly located close to the river mouths. It shows how the different
375   parametrizations of the A_T diverge highly at low salinities. On the other hand, the major differences with Lee et al. (2006) (Fig.
S7b) are surrounding North America's Pacific coast, the area of influence of the Amazon river, the zone between both the
Niger and the Congo rivers and the North Sea. In the open ocean there are some wide areas where the differences are
remarkably high. They are mainly in the South Pacific. It should also be noted that the transition zone between the 1
((sub)tropics) and 2 (equatorial upwelling Pacific) areas defined in the study of Lee et al. (2006) generates a discontinuity in
380   the difference map. Finally, the largest differences with Lauvset et al. (2016) (Fig. S7c) are less localized. The Arctic Ocean
and the Pacific sector of the Southern Ocean are the areas where there is a large continuity in the differences.

An important cause of the different results stems from the use of different inputs to generate the climatologies. As an example,
this can be seen when the climatologies of Lauvset et al. (2016) are used as input variables to compute A_T with the neural
network instead of the WOA13 data. In the surface layer, a considerable reduction of the RMSE (15.7 µmol kg⁻¹ to 12.3 µmol

385 kg^{-1}) and an increase of the r^2 from 0.91 to 0.95 are obtained (Fig. 11). In deeper layers, the differences are progressively decreasing. The values of the RMSE of the comparisons like those in Fig. 11 but below 250m are in the range of 4 to 6 µmol kg^{-1}. In these layers, the improvement caused by the inputs usage is reduced to around 1 µmol kg^{-1}. This result shows an increasing similarity between WOA13 climatologies and Lauvset et al. (2016) climatologies with increasing depth. However, and to be consistent, it is recommended to use the A$_T$ climatology corresponding with the other inputs used in the studies that

390 arise from these products.

4 Data availability

The climatology and the two neural networks designed in this study are available at the data repository of the Spanish National Research Council (CSIC; doi: http://dx.doi.org/10.20350/digitalCSIC/8564).

5 Conclusions

395 A neural network to compute A$_T$ anywhere in the ocean has been presented. As evaluated by the RMSE between the measured and the computed data, the method used in this study offers increased precision compared to previous studies. Furthermore, the global relationship between A$_T$ and input variables was obtained from a higher number of quality-controlled data than before, with a greater temporal and spatial resolution. We have demonstrated how one single global algorithm is able to compute A$_T$ satisfactorily for the entire global ocean. This has enabled us to generate a monthly climatology without the need

400 to use smoothing techniques between different oceanic areas.

The validation using different independent datasets demonstrates the good network generalization. In addition, the spatiotemporal variability of A$_T$ is well captured by the network as shown in time-series validation. Therefore, the obtained climatology using WOA13 inputs should pick up this variability due to the good network performance to new independent data.

405 We offer this global monthly climatology of A$_T$ to the scientific community for advancing the understanding of the ocean carbon cycle. Our new climatology may particularly be useful as input to modeling efforts. It is worthwhile mentioning that the network is also useful to obtain A$_T$ values for samples where the inputs for the neural network are present.

6 Author contributions

DB, FFP and AV designed the study. The manuscript was written by DB and revised and discussed by all the authors. The

410 dataset of the climatology and the neural networks were created by DB.

7 Competing interests

The authors declare that they have no conflict of interest.

8 Acknowledgements

This research was supported by Ministerio de Educación, Cultura y Deporte (FPU grant FPU15/06026), Ministerio de
415   Economía y Competitividad through the ARIOS (CTM2016-76146-C3-1-R) project co-funded by the Fondo Europeo de
Desarrollo Regional 2014-2020 (FEDER) and EU Horizon 2020 through the AtlantOS project (grant agreement 633211). The
authors want to thank the comments of Siv K. Lauvset to improve the manuscript.

9 References

Anderson, L. G., Jutterström, S., Kaltin, S., Jones, E. P. and Björk, G.: Variability in river runoff distribution in the Eurasian
420   Basin of the Arctic Ocean, J. Geophys. Res., 109(C1), 1–8, doi:10.1029/2003JC001773, 2004.

Artioli, Y., Blackford, J. C., Butenschön, M., Holt, J. T., Wakelin, S. L., Thomas, H., Borges, A. V and Allen, I.: The
carbonate system in the North Sea: sensitivity and model validation, J. Mar. Syst., 102–104, 1–13,
doi:10.1016/j.jmarsys.2012.04.006, 2012.

Bakker, D. C. E., Pfeil, B., Landa, C. S., Metzl, N., O'Brien, K. M., Olsen, A., Smith, K., Cosca, C., Harasawa, S., Jones, S.
425   D., Nakaoka, S. I., Nojiri, Y., Schuster, U., Steinhoff, T., Sweeney, C., Takahashi, T., Tilbrook, B., Wada, C., Wanninkhof,
R., Alin, S. R., Balestrini, C. F., Barbero, L., Bates, N. R., Bianchi, A. A., Bonou, F., Boutin, J., Bozec, Y., Burger, E. F.,
Cai, W. J., Castle, R. D., Chen, L., Chierici, M., Currie, K., Evans, W., Featherstone, C., Feely, R. A., Fransson, A., Goyet,
C., Greenwood, N., Gregor, L., Hankin, S., Hardman-Mountford, N. J., Harlay, J., Hauck, J., Hoppema, M., Humphreys, M.
P., Hunt, C. W., Huss, B., Ibánhez, J. S. P., Johannessen, T., Keeling, R., Kitidis, V., Körtzinger, A., Kozyr, A.,
430   Krasakopoulou, E., Kuwata, A., Landschützer, P., Lauvset, S. K., Lefèvre, N., Lo Monaco, C., Manke, A., Mathis, J. T.,
Merlivat, L., Millero, F. J., Monteiro, P. M. S., Munro, D. R., Murata, A., Newberger, T., Omar, A. M., Ono, T., Paterson,
K., Pearce, D., Pierrot, D., Robbins, L. L., Saito, S., Salisbury, J., Schlitzer, R., Schneider, B., Schweitzer, R., Sieger, R.,
Skjelvan, I., Sullivan, K. F., Sutherland, S. C., Sutton, A. J., Tadokoro, K., Telszewski, M., Tuma, M., Van Heuven, S. M. A.
C., Vandemark, D., Ward, B., Watson, A. J. and Xu, S.: A multi-decade record of high-quality fCO2 data in version 3 of the
435   Surface Ocean CO2 Atlas (SOCAT), Earth Syst. Sci. Data, 8(2), 383–413, doi:10.5194/essd-8-383-2016, 2016.

Bates, N., Astor, Y., Church, M., Currie, K., Dore, J., Gonazález-Dávila, M., Lorenzoni, L., Muller-Karger, F., Olafsson, J.
and Santana-Casiano, M.: A Time-Series View of Changing Ocean Chemistry Due to Ocean Uptake of Anthropogenic CO2
and Ocean Acidification, Oceanography, 27(1), 126–141, doi:10.5670/oceanog.2014.16, 2014.

Brewer, P. G. and Goldman, J. C.: Alkalinity changes generated by phytoplankton, Limnol. Oceanogr., 21(1), 108–117,

440   doi:10.4319/lo.1976.21.1.0108, 1976.

Carter, B. R., Williams, N. L., Gray, A. R. and Feely, R. A.: Locally interpolated alkalinity regression for global alkalinity estimation, Limnol. Oceanogr. Methods, 14(4), 268–277, doi:10.1002/lom3.10087, 2016.

Cooper, L. W., McClelland, J. W., Holmes, R. M., Raymond, P. A., Gibson, J. J., Guay, C. K. and Peterson, B. J.: Flow-weighted values of runoff tracers (δ18O, DOC, Ba, alkalinity) from the six largest Arctic rivers, Geophys. Res. Lett., 35(18),
445   3–7, doi:10.1029/2008GL035007, 2008.

Fabry, V. J., Seibel, B. A., Feely, R. A., Fabry, J. C. O. and Fabry, V. J.: Impacts of ocean acidification on marine fauna and ecosystem processes, ICES J. Mar. Sci., 65(December), 414–432, doi:10.1093/icesjms/fsn048, 2008.

Fine, R. A., Willey, D. A. and Millero, F. J.: Alkalinity from Aquarius satellite data, Geophys. Res. Lett., 44, 261–267, doi:10.1002/2016GL071712, 2017.

450   Fry, C. H., Tyrrell, T., Hain, M. P., Bates, N. R. and Achterberg, E. P.: Analysis of global surface ocean alkalinity to determine controlling processes, Mar. Chem., 174, 46–57, doi:10.1016/j.marchem.2015.05.003, 2015.

Gardner, M. . and Dorling, S. .: Artificial neural networks (the multilayer perceptron)—a review of applications in the atmospheric sciences, Atmos. Environ., 32(14–15), 2627–2636, doi:10.1016/S1352-2310(97)00447-0, 1998.

Gevrey, M., Dimopoulos, I. and Lek, S.: Review and comparison of methods to study the contribution of v ariables in
455   artificial neural network models, Ecol. Modell., 160, 249–264, 2003.

Hagan, M. T., Demuth, H. B., Beale, M. H. and De Jesús, O.: Neural network design. ISBN 978-0971732117, 2014.

Hoegh-Guldberg, O. and Bruno, J. F.: The Impact of Climate Change on the World's Marine Ecosystems, Science (80-.)., 328(5985), 1523-1528 doi:10.1126/science.1189930, 2010.

Hoppema, M.: The distribution and seasonal variation of alkalinity in the Southern Bight of the North Sea and in the Western
460   Wadden Sea, Netherlands J. Sea Res., 26(1), 11–23, doi:10.1016/0077-7579(90)90053-J, 1990.

Key, R. M., Olsen, A., van Heuven, S., Lauvset, S. K., Velo, A., Lin, X., Schirnick, C., Kozyr, A., Tanhua, T., Hoppema, M., Jutterström, S., Steinfeldt, R., Jeansson, E., Ishi, M., Perez, F. F. and Suzuki, T.: Global Ocean Data Analysis Project, Version 2 (GLODAPv2), ORNL/CDIAC-162, NDP-093, doi:10.3334/CDIAC/OTG.NDP093_GLODAPv2, 2015.

Kim, H. and Lee, K.: Significant contribution of dissolved organic matter to seawater alkalinity, Geophys. Res. Lett.,

465   36(September), 1–5, doi:10.1029/2009GL040271, 2009.

Kroeker, K. J., Kordas, R. L., Crim, R., Hendriks, I. E., Ramajo, L., Singh, G. S., Duarte, C. M. and Gattuso, J.-P.: Impacts of ocean acidification on marine organisms: quantifying sensitivities and interaction with warming, Glob. Chang. Biol., 19(6), 1884–1896, doi:10.1111/gcb.12179, 2013.

Landschützer, P., Gruber, N., Bakker, D. C. E., Schuster, U., Nakaoka, S., Payne, M. R., Sasse, T. P. and Zeng, J.: A neural

470   network-based estimate of the seasonal to inter-annual variability of the Atlantic Ocean carbon sink, Biogeosciences, 10(11), 7793–7815, doi:10.5194/bg-10-7793-2013, 2013.

Landschützer, P., Gruber, N., Bakker, D. C. E. and Schuster, U.: Recent variability of the global ocean carbon sink, Global Biogeochem. Cycles, 28(9), 927–949, doi:10.1002/2014GB004853, 2014.

Lauvset, S. K., Key, R. M., Olsen, A., Van Heuven, S., Velo, A., Lin, X., Schirnick, C., Kozyr, A., Tanhua, T., Hoppema,

475   M., Jutterström, S., Steinfeldt, R., Jeansson, E., Ishii, M., Perez, F. F., Suzuki, T. and Watelet, S.: A new global interior ocean mapped climatology: The $1° \times 1°$ GLODAP version 2, Earth Syst. Sci. Data, 8(2), 325–340, doi:10.5194/essd-8-325-2016, 2016.

Levenberg, K.: A Method for the solution of certain non-linear probles in least squares., Q. Appl. Math., II(2), 164–168, 1944.

480   MacKay, D. J. C.: Bayesian Interpolation, Neural Comput., 4(3), 415–447, doi:10.1162/neco.1992.4.3.415, 1992.

Marquardt, D.: An Algorithm for Least-Squares Estimation of Nonlinear Parameters, J. Soc. Ind. Appl. Math., 11(2), 1963.

Millero, F. J., Lee, K. and Roche, M.: Distribution of alkalinity in the surface waters of the major oceans, Mar. Chem., 60(1–2), 111–130, doi:10.1016/S0304-4203(97)00084-4, 1998.

Olden, J. D. and Jackson, D. A.: Illuminating the "' black box '": a randomization approach for understanding variable

485   contributions in artificial neural networks, Ecol. Modell., 154, 135–150, doi:10.1016/S0304-3800(02)00064-9, 2002.

Olden, J. D., Joy, M. K. and Death, R. G.: An accurate comparison of methods for quantifying variable importance in artificial neural networks using simulated data An accurate comparison of methods for quantifying variable importance in artificial neural networks using simulated data, Ecol. Modell., 178, 389–397, doi:10.1016/j.ecolmodel.2004.03.013, 2004.

Olsen, A., Key, R. M., Van Heuven, S., Lauvset, S. K., Velo, A., Lin, X., Schirnick, C., Kozyr, A., Tanhua, T., Hoppema,

490   M., Jutterström, S., Steinfeldt, R., Jeansson, E., Ishii, M., Pérez, F. F. and Suzuki, T.: The global ocean data analysis project

version 2 (GLODAPv2) - An internally consistent data product for the world ocean, Earth Syst. Sci. Data, 8(2), 297–323, doi:10.5194/essd-8-297-2016, 2016.

Orr, J. C., Fabry, V. J., Aumont, O., Bopp, L., Doney, S. C., Feely, R. A., Gnanadesikan, A., Gruber, N., Ishida, A., Joos, F., Key, R. M., Lindsay, K., Maier-Reimer, E., Matear, R., Monfray, P., Mouchet, A., Najjar, R. G., Plattner, G. K., Rodgers, K. B., Sabine, C. L., Sarmiento, J. L., Schlitzer, R., Slater, R. D., Totterdell, I. J., Weirig, M. F., Yamanaka, Y. and Yool, A.: Anthropogenic ocean acidification over the twenty-first century and its impact on calcifying organisms, Nature, 437(7059), 681–686, 2005.

Le Quéré, C., Andrew, R. M., Friedlingstein, P., Sitch, S., Pongratz, J., Manning, A. C., Korsbakken, J. I., Peters, G. P., Canadell, J. G., Jackson, R. B., Boden, T. A., Tans, P. P., Andrews, O. D., Arora, V. K., Bakker, D. C. E., Barbero, L., Becker, M., Betts, R. A., Bopp, L., Chevallier, F., Chini, L. P., Ciais, P., Cosca, C. E., Cross, J., Currie, K., Gasser, T., Harris, I., Hauck, J., Haverd, V., Houghton, R. A., Hunt, C. W., Hurtt, G., Ilyina, T., Jain, A. K., Kato, E., Kautz, M., Keeling, R. F., Klein Goldewijk, K., Körtzinger, A., Landschützer, P., Lefèvre, N., Lenton, A., Lienert, S., Lima, I., Lombardozzi, D., Metzl, N., Millero, F., Monteiro, P. M. S., Munro, D. R., Nabel, J. E. M. S., Nakaoka, S., Nojiri, Y., Padín, X. A., Peregon, A., Pfeil, B., Pierrot, D., Poulter, B., Rehder, G., Reimer, J., Rödenbeck, C., Schwinger, J., Séférian, R., Skjelvan, I., Stocker, B. D., Tian, H., Tilbrook, B., van der Laan-Luijkx, I. T., van der Werf, G. R., van Heuven, S., Viovy, N., Vuichard, N., Walker, A. P., Watson, A. J., Wiltshire, A. J., Zaehle, S. and Zhu, D.: Global Carbon Budget 2017, Earth Syst. Sci. Data Discuss., 1–79, doi:10.5194/essd-2017-123, 2017.

Rumelhart, D. E., Hinton, G. E. and Williams, R. J.: Learning representations by back-propagating errors, Nature, 323(6088), 533–536, doi:10.1038/323533a0, 1986.

Russell, S. J. and Norvig, P.: Artificial intelligence : a modern approach, Prentice Hall., 2010.

Sauzède, R., Claustre, H., Pasqueron de Fommervault, O., Bittig, H. C., Gattuso, J.-P., Legendre, L. and Johnson, K. S.: Estimates of water-column nutrients concentration and carbonate system parameters in the global ocean: A novel approach based on neural networks, Front. Mar. Sci., 4(May), 1–17, doi:10.3389/fmars.2017.00128, 2017.

Takahashi, T., Sutherland, S. C., Chipman, D. W., Goddard, J. G. and Ho, C.: Climatological distributions of pH, pCO2, total CO2, alkalinity, and CaCO3 saturation in the global surface ocean, and temporal changes at selected locations, Mar. Chem., 164, 95–125, doi:10.1016/j.marchem.2014.06.004, 2014.

Tanhua, T., Bates, N. R. and Körtzinger, A.: The marine carbon cycle and ocean carbon inventories, Int. Geophys., 103, 787–815, doi:10.1016/B978-0-12-391851-2.00030-1, 2013.

Troupin, C., Machín, F., Ouberdous, M., Sirjacobs, D., Barth, A. and Beckers, J.-M.: High-resolution climatology of the
520 northeast Atlantic using Data-Interpolating Variational Analysis (Diva), J. Geophys. Res. Ocean., 115(C8), 1–20,
doi:10.1029/2009JC005512, 2010

Vázquez-Rodríguez, M., Padin, X. A., Pardo, P. C., Ríos, A. F. and Pérez, F. F.: The subsurface layer reference to calculate
preformed alkalinity and air-sea CO2 disequilibrium in the Atlantic Ocean, J. Mar. Syst., 94, 52–63,
doi:10.1016/j.jmarsys.2011.10.008, 2012.

525 Velo, A., Pérez, F. F., Tanhua, T., Gilcoto, M., Ríos, A. F. and Key, R. M.: Total alkalinity estimation using MLR and neural
network techniques, J. Mar. Syst., 111–112, 11–18, doi:10.1016/j.jmarsys.2012.09.002, 2013.

Wolf-Gladrow, D. A., Zeebe, R. E., Klaas, C., Körtzinger, A. and Dickson, A. G.: Total alkalinity: The explicit conservative
expression and its application to biogeochemical processes, Mar. Chem., 106(1–2 SPEC. ISS.), 287–300,
doi:10.1016/j.marchem.2007.01.006, 2007.

530 Zeng, J., Nojiri, Y., Landschützer, P., Telszewski, M. and Nakaoka, S.: A global surface ocean fCO2 climatology based on a
feed-forward neural network, J. Atmos. Ocean. Technol., 31(8), 1838–1849, doi:10.1175/JTECH-D-13-00137.1, 2014.

Zweng, M.M, Reagan, J.R., Antonov, J.I., Locarnini, R.A., Mishonov, A.V., Boyer, T.P., Garcia, H.E., Baranova, O.K.,
Johnson, D.R., Seidov, D. and Biddle M.M. World Ocean Atlas 2013, Volume 2: Salinity. S. Levitus, Ed., A. Mishonov
Technical Ed.; NOAA Atlas NESDIS 74, 39 pp, 2013.

535

$$A_T = f^2 (W^2 f^1 (W^1 p + b^1) + b^2)$$
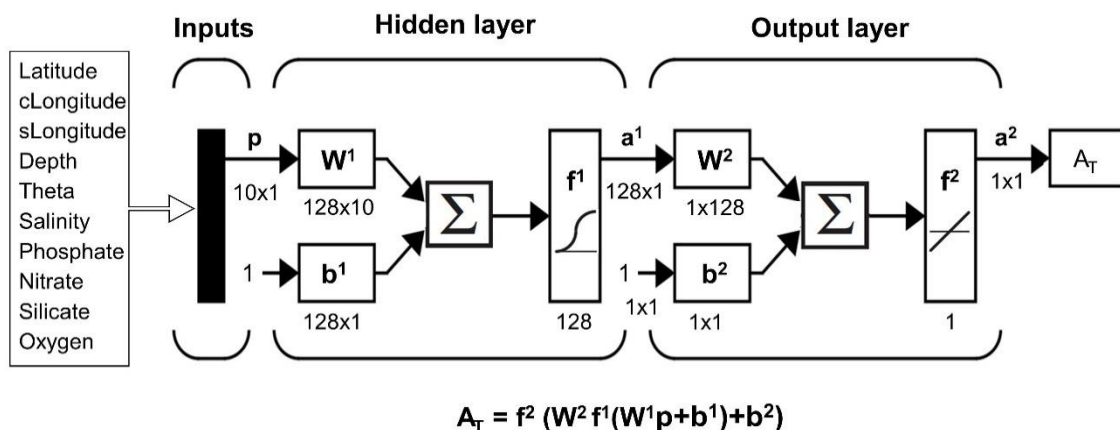
Figure 1: Neural network configuration. The notation is in agreement with Hagan et al. (2014). Theta: potential temperature; p: input vectors; W: weight matrix; b: bias matrix; ∑: sum; f: transfer function; a: output matrix. The superscripts indicate de number of the layer. The c and s preceding month and longitude variables represent cosine and sine (See equations below)). The dimensions of the matrices are for an individual sample. Modified from Hagan et al. (2014).

540
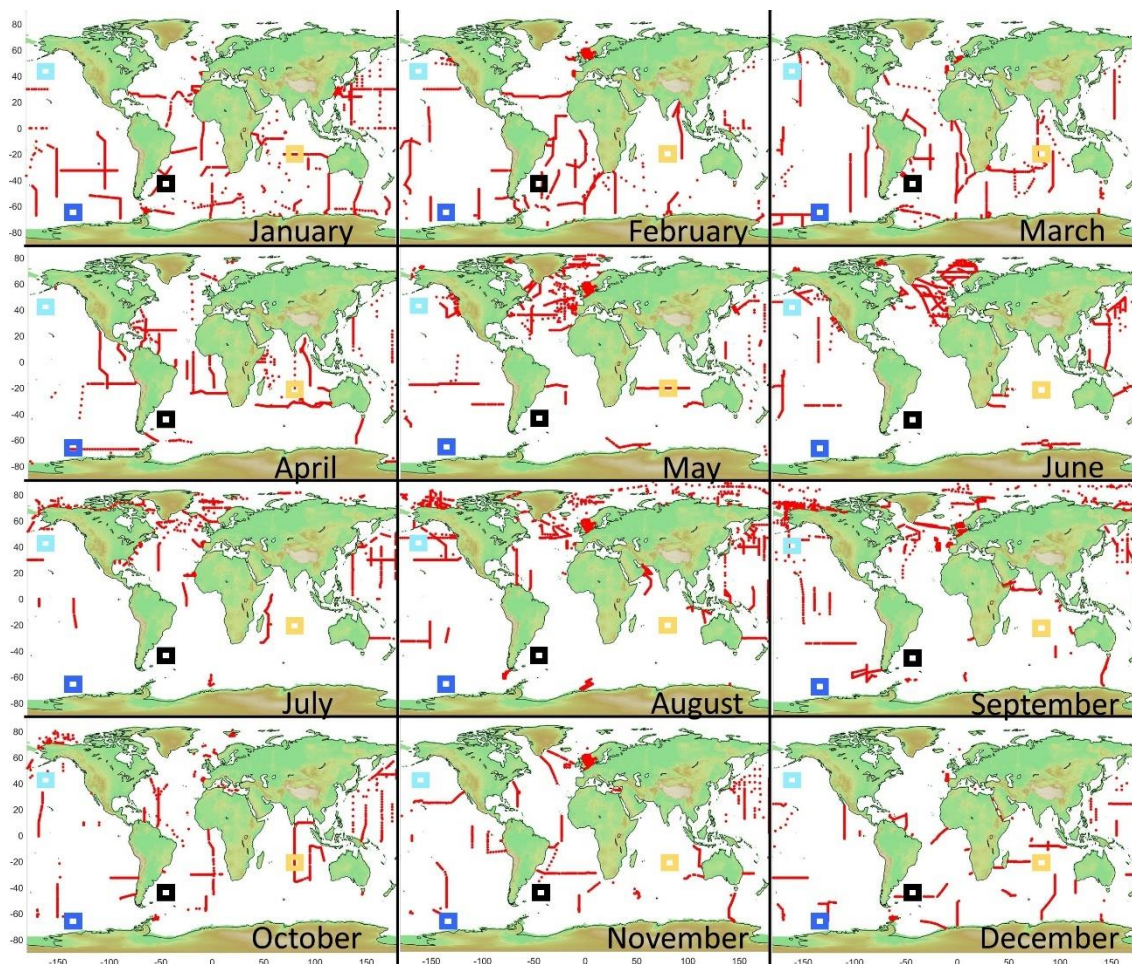
Figure 2: Red dots: locations of GLODAPv2 data used in this study. Colored rectangles: areas where subsurface layer hypothesis was evaluated. The areas were chosen based on the non-availability of A_T data in two or more consecutive months in the same oceanographic regime as the colored area.

545
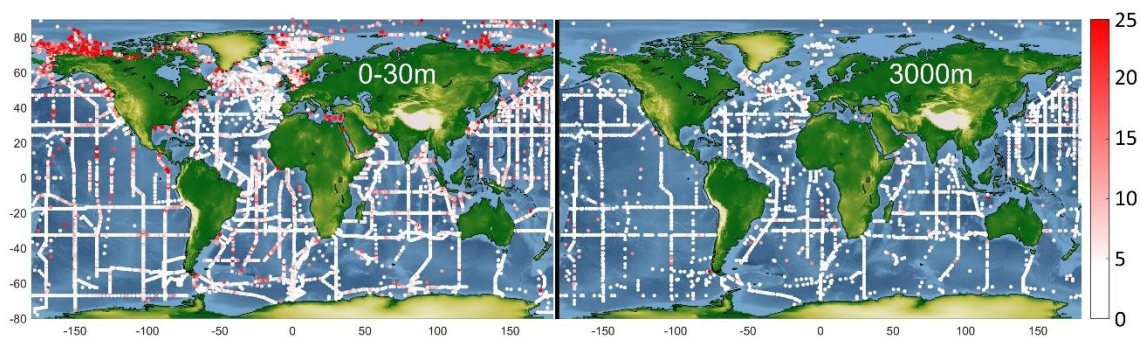
Figure 3: Absolute differences between GLODAPv2 A$_T$ and NN A$_T$. Left: samples in the layer 0-30m. Right: samples in the layer 2950-3050m.
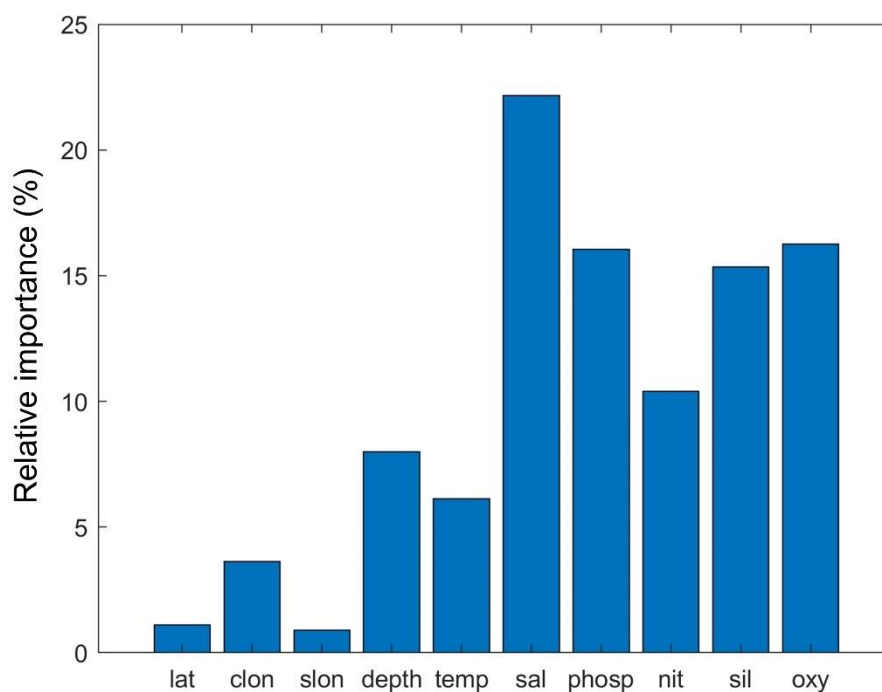
Figure 4: Relative importance of the predictor variables for the NN. lat: latitude; clon: cos (longitude); slon: (sin (longitude);
550 **temp: temperature; sal: salinity; phosp: phosphate; nit: nitrate; sil: silicate; oxy: oxygen.**
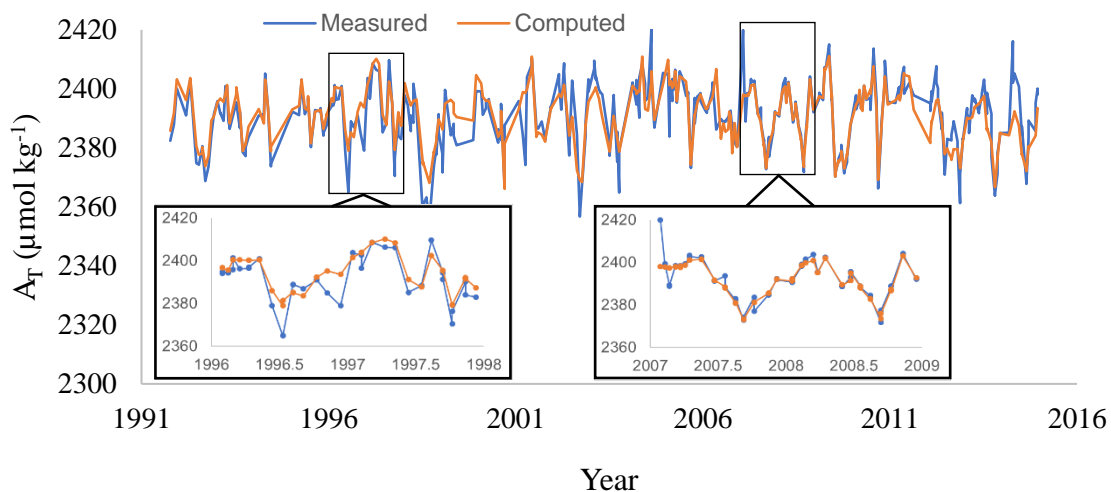
Figure 5: Comparison of measured and computed A$_T$ for the depth range 0-10 m at time-series station BATS. RMSE: 5.7 µmol kg^{-1}. The years 1996-1997 and 2007-2008 are amplified to show the monthly variations because they are the years with A$_T$ measurements in all the months.
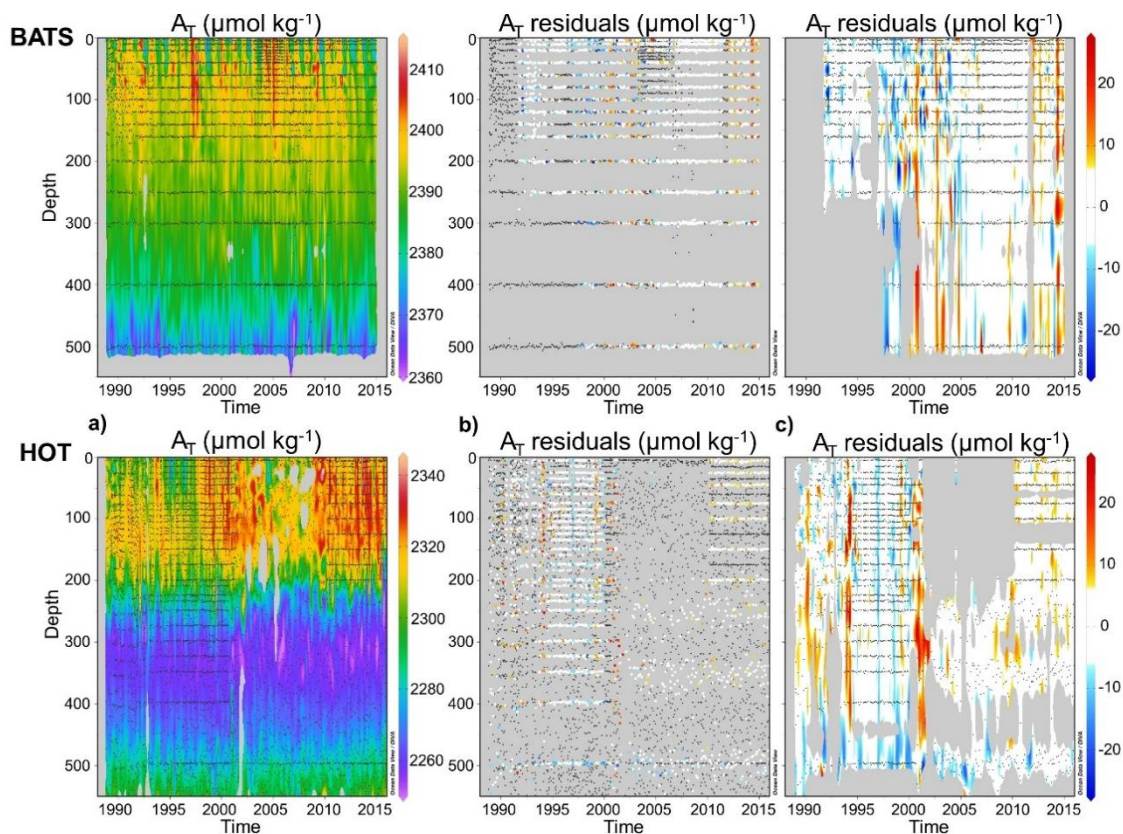
555

Figure 6: a) Computed A$_T$ for the upper 550m of the water column at the BATS and HOT time-series stations. b) Difference between measured and computed A$_T$. Colored dots show samples where A$_T$ was measured. Black dots show samples where A$_T$ was not measured but the network inputs were. c) Difference between measured and computed A$_T$ interpolated with Data-Interpolating Variational Analysis (DIVA; Troupin et al., 2010). This figure was made with Ocean Data View (Schlitzer, 2016).

560
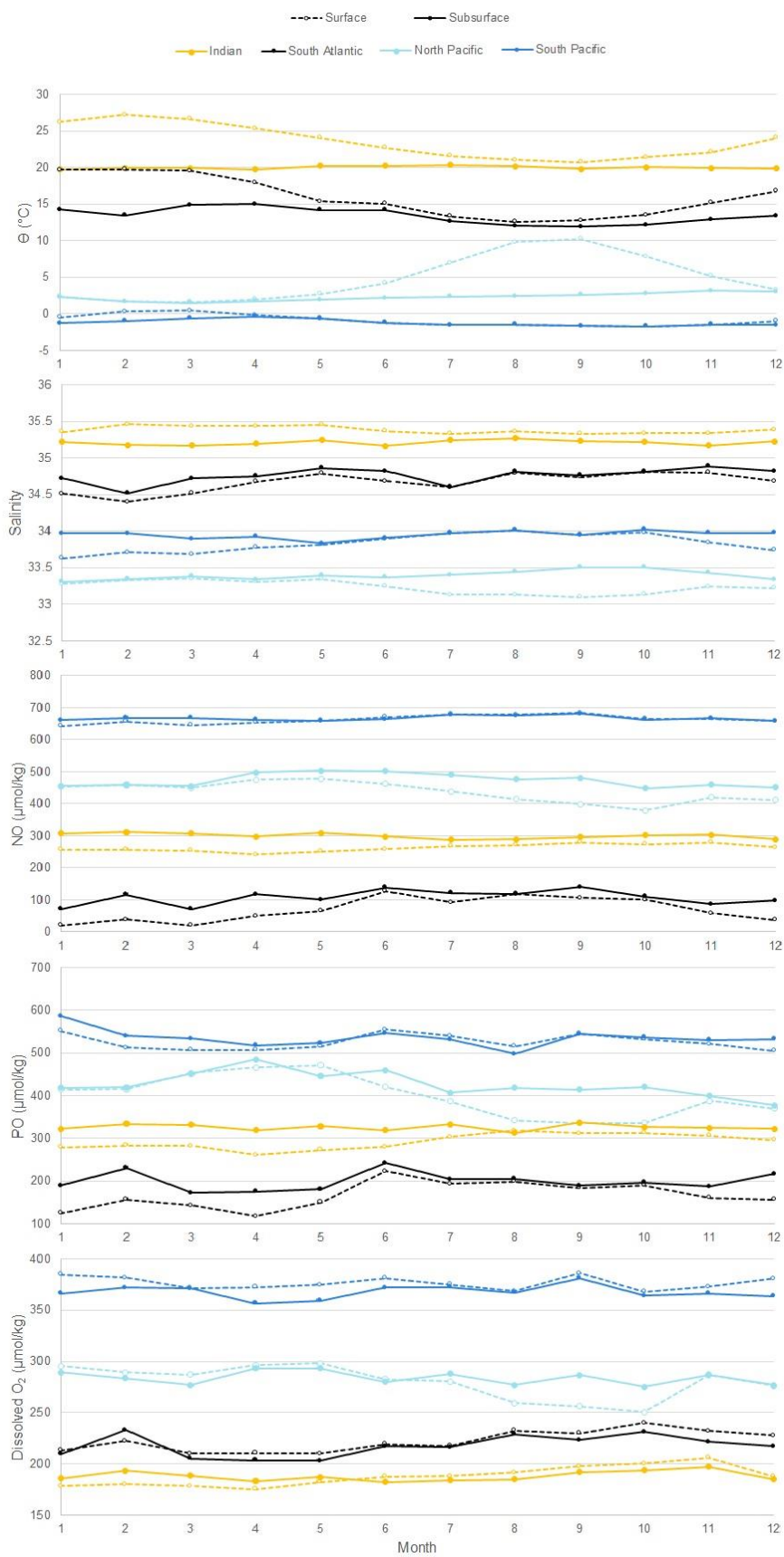
Figure 7: Monthly variability of Θ (potential temperature), salinity, NO = 9*NO₃ + O₂ and PO = 135*PO₄ + O₂ (defined according to Broecker, 1974) for different ocean basins. Data from WOA13 objectively analyzed monthly climatologies were averaged for each area defined in Figure 2. Each zone is displaced in each graph for a certain constant quantity of the variable for a better visualization, that is, the data shown are not the real values. Indian Ocean: 100-200m; South Atlantic, South Pacific and North Pacific: 50-100m.
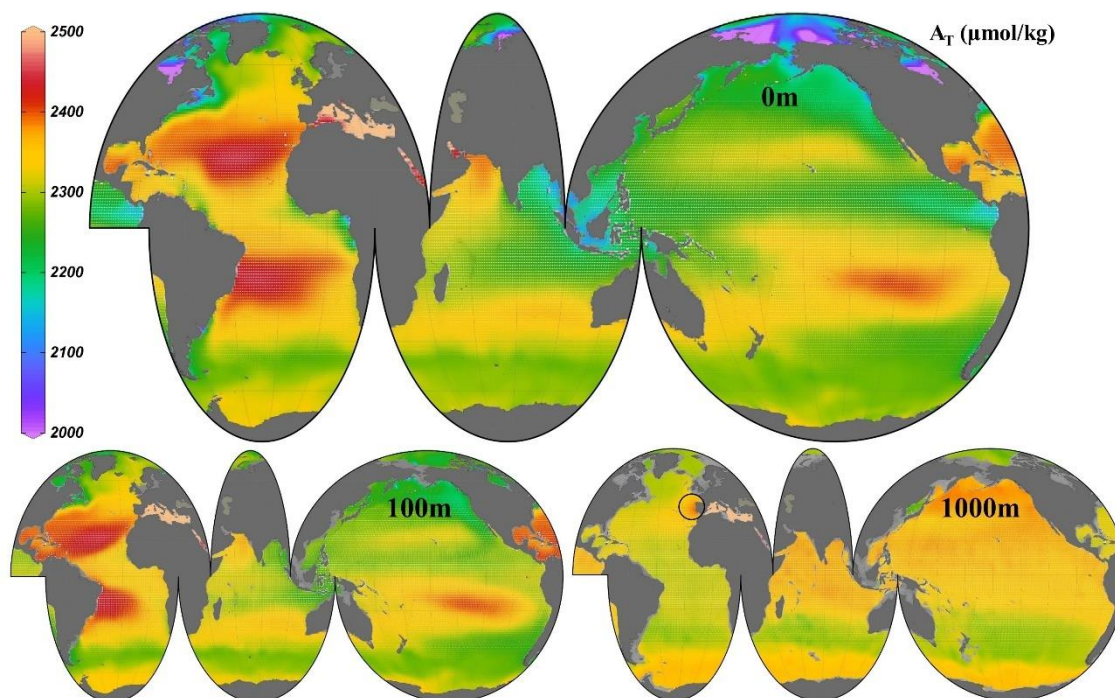
Figure 8: Annual mean climatology of A_T at 3 depths. Black circle in 1000m panel points out the area of influence of the Mediterranean Water in the Atlantic Ocean. This figure was made with Ocean Data View (Schlitzer, 2016).
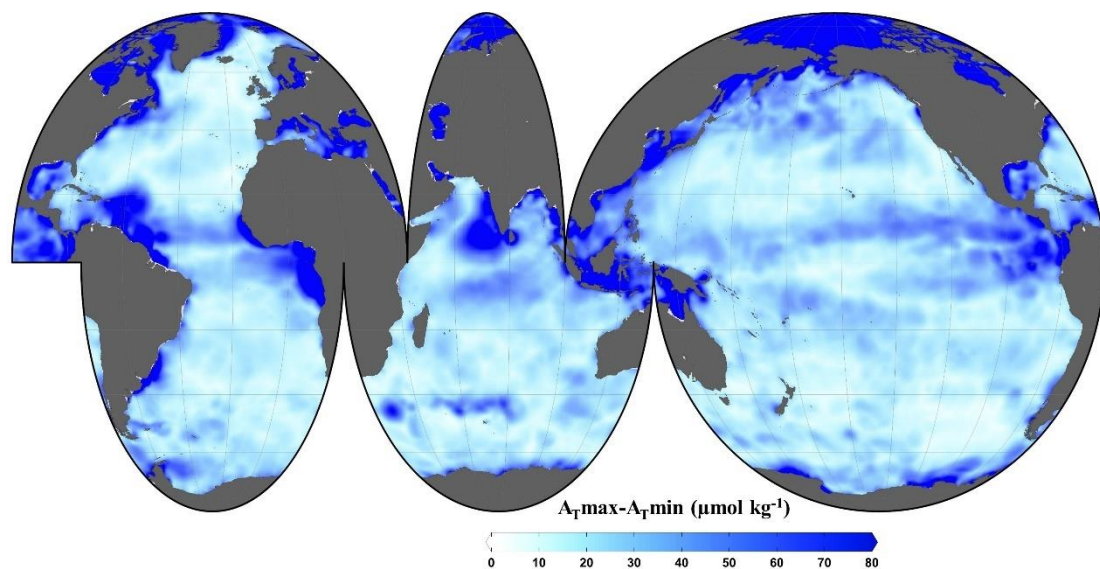
570

Figure 9: Seasonal amplitude of sea surface A_T. This figure was made with Ocean Data View (Schlitzer, 2016).
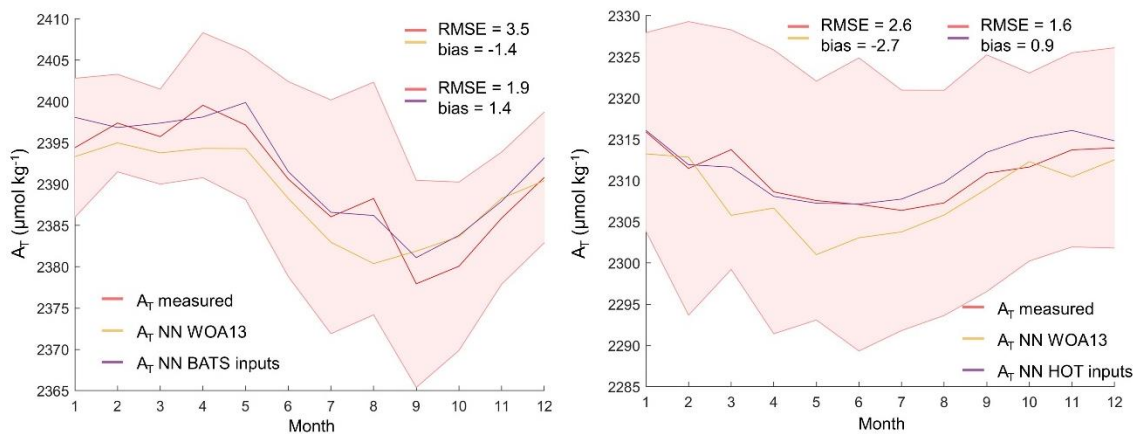
Figure 10: Climatology of A_T from measured data, from NN using measured data as inputs and from NN using WOA13 data as inputs at BATS (0-5 m; left panel) and HOT (0-30 m; right panel) time-series location. The shading represents the standard deviation
575 **of the average of the measured data. Units of RMSE and bias are µmol kg⁻¹**
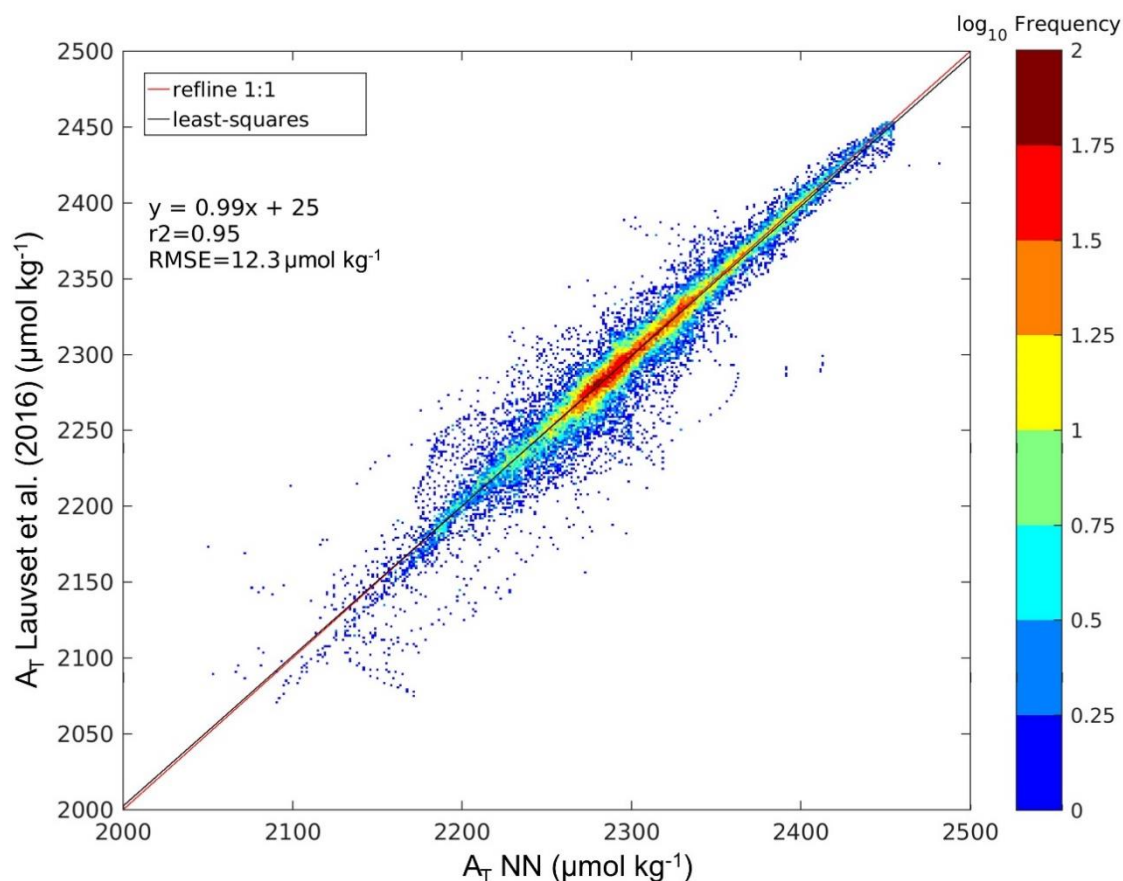
Figure 11: Regression between A_T computed with NN applied on the climatologies of Lauvset et at. (2016) and A_T from Lauvset et at. (2016) at 0m. The graph is divided in pixels. The color of each pixel is determined by the number of points inside it. Note the logarithmic scale to account for the large amount of data.

Approach	RMSE (μmol kg^{-1})	bias (μmol kg^{-1})	n
NN_GLODAPv2 (lm)	8.2	0.02	246221
NN_GLODAPv2 (br)	8	0.03	246221
NN_GLODAPv2w3RMSE (lm)	5.1	-0.002	243754
NNw3RMSE_GLODAPv2w3RMSE (lm)	4.8	-0.006	243754

580 **Table 1: The RMSE between GLODAPv2 A_T and A_T computed by the neural network. n: number of samples. NN: neural network trained with the initial dataset. NNw3RMSE: neural network trained with the dataset without samples with residuals beyond ±3RMSE. GLODAPv2: initial dataset. GLODAPv2w3RMSE: dataset without samples with residuals beyond ±3RMSE. lm: Levenberg-Marquardt. br: Bayesian Regularization**

Areas defined in Lee et al. (2006)	RMSE			n
	Lee et al. (2006)	NN	NNw3RMSE	
North Atlantic	13.5	12.3	**12.1**	2765
North Pacific	16.8	10.5	**9.6**	2087
Equatorial Upwelling Pacific	7.8	9.5	**5.7**	481
Subtropics	20.8	**15.1**	15.2	4309
Southern Ocean	10.1	5.9	**5.3**	3610
Weighted RMSE	15.3	11.1	**10.6**	13252

Table 2: RMSE obtained by the relations of Lee et al. (2006), NN and NNw3RMSE over GLODAPv2. In bold the lowest RMSE in each area defined in Lee et al. (2006). To be consistent with the surface layer defined in Lee et al. (2006) the samples evaluated here are from above 20m (subtropics) and 30m (the rest).

Areas defined in Takahashi et al. (2014)	RMSE (µmol kg-1)			n
	Takahashi et al. (2014)	NN	NNw3RMSE	
West GIN Seas	29.2	**10.4**	11.8	623
East GIN Seas	11.6	9.5	**9.0**	990
High Arctic	24.9	**15.2**	16.2	594
Beaufort Sea	57.6	**46.9**	79.3	2086
Labrador Sea	27.7	22.7	**22.1**	736
Subarctic Atlantic	15.6	**10.4**	11.3	1041
North Atlantic Drift	7.7	7.9	**7.2**	1403
Central Atlantic	23.1	**19.9**	20.1	3276
South Atlantic Transition Zone	6.7	6.8	**5.9**	291
Antarctic (Atlantic)	7.5	5.8	**5.2**	727
Kuroshio-Alaska Gyre	16.2	10.8	**9.8**	1412
North Central Pacific	13.2	10.0	**9.4**	1224
Okhotsk Sea	**5.4**	7.8	**5.4**	20
Central Tropical North Pacific	9.3	7.3	**7.0**	1328
Tropical East North Pacific	30.9	11.2	**10.3**	308
Panama Basin	8.1	13.4	**7.4**	58
Central South Pacific	9.7	6.4	**5.8**	2834
East Central South Pacific	11.6	9.3	**8.8**	249
Subpolar South Pacific	8.2	5.2	**4.6**	431
Antarctic (Pacific)	4.9	4.3	**3.0**	524
Main North Indian	7.0	6.2	**4.6**	493
Red Sea	**6.3**	9.3	9.2	19
Bengal Basin	8.9	7.8	**6.3**	96
Main South Indian	8.8	7.1	**6.8**	2536
South Indian Transition	7.9	5.4	**3.8**	330
Antarctic (Indian)	8.1	5.0	**4.0**	865

Circumpolar Southern Ocean	10.1	5.9	**5.3**	1970
Weighted RMSE	17.0	**12.8**	15.0	26464
Weighted RMSE without Beaufort Sea	13.5	9.9	**9.5**	24378

Table 3: RMSE obtained by the relations of Takahashi et al. (2014), NN and NNw3RMSE over GLODAPv2. In bold, the lowest RMSE in each area defined in Takahashi et al. (2014). To be consistent with the surface layer defined in Takahashi et al. (2014) the samples evaluated here are from above 50m.

Time-Series	Location	RMSE (μmol kg^{-1})	bias (μmol kg^{-1})	r^2	n
HOT	22º45'N, 158º00'W	**5.9**	**-0.80**	**0.99**	3853
BATS	31º40'N, 64º10'W	**6.2**	**-0.18**	**0.77**	3033
ESTOC	29º10'N, 15º30'W	**3.3**	**0.64**	**0.99**	1700
KNOT	44ºN, 155ºE	**4.7**	**-6.40**	**0.996**	1234
K2	47ºN, 160E	**3.1**	**-3.03**	**0.998**	561

Table 4: RMSE between measured A$_T$ and neural network computed A$_T$. r^2 from the measured A$_T$ vs computed A$_T$ regression. The comparison was done for all the samples where the input variables and the A$_T$ were measured in the same water sample.

RMSE (μmol kg^{-1})\r^2	NN	Lauvset et al. 2016*	Takahashi et al. 2014	Lee et al. 2006
NN		0.91	0.92	0.97
Lauvset et al. 2016*	15.7		0.90	0.92
Takahashi et al. 2014	15.3	17.8		0.93
Lee et al. 2006	8.0	14.6	12.4	

Table 5: Comparison of four annual mean surface climatologies of A$_T$. *The Arctic Ocean and the Baltic Sea are not included in the comparisons for coherency reasons.

Month	Lee et al. (2006) vs NN		Takahashi et al. (2014) vs NN		Lee et al. (2006) vs Takahashi et al. (2014)	
	RMSE (μmol kg^{-1})	r2	RMSE (μmol kg^{-1})	r2	RMSE (μmol kg^{-1})	r2
January	12.6	0.93	18.5	0.89	14.2	0.92
February	12.2	0.94	24.2	0.82	14.7	0.91
March	12.1	0.94	19.5	0.87	14.3	0.91
April	12.1	0.94	18.4	0.88	15.0	0.91
May	12.4	0.93	19.0	0.86	13.8	0.92
June	12.7	0.93	17.7	0.89	14.3	0.91
July	12.3	0.93	24.9	0.84	14.8	0.91
August	12.9	0.93	19.5	0.89	14.8	0.91
September	12.5	0.93	17.9	0.91	14.9	0.91
October	11.9	0.94	20.8	0.88	13.1	0.93
November	12.0	0.94	27.9	0.80	12.8	0.93
December	11.7	0.94	18.9	0.89	13.9	0.92

595   **Table 6: Comparison between the three monthly climatologies of A_T.**